Theory of (001) surface and bulk states in $Y_{1-y}Ca_yBa_2Cu_3O_{7-\delta}$

K. Pasanai[1,2] and W. A. Atkinson[2,*]

[1]*School of Physics, Institute of Science, Suranaree University of Technology, 111 University Avenue, Muang District, Nakhon Ratchasima 30000, Thailand*

[2]*Trent University, 1600 West Bank Drive, Peterborough, Ontario, Canada K9J 7B8*

(Received 15 January 2010; revised manuscript received 12 March 2010; published 1 April 2010)

A self-consistent model is developed for the surface and bulk states of thin $Y_{1-y}Ca_yBa_2Cu_3O_{7-\delta}$(YCBCO) films. The dispersions of the chain and plane layers are modeled by tight-binding bands, and the electronic structure is then calculated for a finite-thickness film. The dopant atoms are treated within a virtual crystal approximation. Because YCBCO is a polar material, self-consistent treatment of the long range Coulomb interaction leads to a transfer of charge to the film surfaces, and to the formation of surface states. The tight-binding band parameters are constrained by the requirement that the calculated band structure of surface states at CuO_2-terminated surfaces be in agreement with photoemission experiments. The spectral function and density of states are calculated and compared with experiments. Unlike the case of $Bi_2Sr_2CaCu_2O_8$, where the surfaces are believed to be representative of the bulk, the densities of states at the YCBCO surfaces are shown to be qualitatively different from the bulk, and are sensitive to doping. The calculated spectral function agrees closely with both bulk-sensitive and surface-sensitive photoemission results, while the calculated density of states for optimally doped YCBCO agrees closely with tunneling experiments. We find that some density of states features previously ascribed to competing order can be understood as band structure effects.

DOI: 10.1103/PhysRevB.81.134501 PACS number(s): 74.55.+v, 74.72.Gh, 74.25.Jb

I. INTRODUCTION

The density of states (DOS) measured by tunneling experiments in the $YBa_2Cu_3O_{7-\delta}$ (YBCO) family of high temperature superconductors is complicated. Several experiments on superconducting samples have measured densities of states with multiple energy scales.[1–7] Some experiments find a subgap feature[3,4] while others do not,[2,5,6,8] and all experiments near optimal doping find satellite features at energies larger than the gap energy. Many of these studies find that the spectra change qualitatively with doping and can vary significantly at different points on the sample surface.[4,6] Spectral features have been interpreted in terms of band structure,[4] competing order,[6,9] and coupling to bosonic modes.[5]

In this work, we explore reasons why the YBCO single-particle spectrum is so complicated, particularly when compared to that of the related superconductor $Bi_2Sr_2CaCu_2O_8$ (BSCCO).[10–12] In BSCCO, there is a clear *d*-wave-like gap in the density of states, and it has been possible to reproducibly extract detailed information about the band structure[7,13,14] and superconducting state.[15,16] At present, there is no consensus on how to interpret the tunneling DOS in YBCO. In this work, we focus on two specific structural differences between BSCCO and YBCO, namely, that YBCO is a polar material while BSCCO is not, and that YBCO has conducting one-dimensional CuO chains while BSCCO does not. We show that the confluence of these two factors explains some features of the experimentally measured DOS. In particular, our results suggest that some features that were previously thought to indicate charge-ordering actually come from peculiarities of the YBCO band structure.

The polarity of the YBCO unit cell is important for several reasons. Unlike BSCCO, YBCO has no natural cleavage plane (i.e., no plane along which ionic forces vanish), making it difficult to prepare surfaces that are clean enough for experiments. More importantly for this work, there is a charge transfer to the YBCO surfaces as a result of the electric fields generated by the polar unit cell. This charge transfer leads to the formation of surface states that can differ significantly from states in the bulk. In contrast, it is widely believed that the surface layers in BSCCO are representative of the bulk.

Surface charging in polar crystals has recently become prominent in the context of $LaAlO_3/SrTiO_3$ interfaces.[17,18] The essential idea is that, since the opposite faces of a polar unit cell have opposite charge, there is a potential difference between them. In a thin film, the potential difference between the top and bottom surfaces of the film is equal to the potential difference across a single unit cell times the number of unit cells spanning the film. The potential difference between the surfaces of the film is thus proportional to the film thickness, much like a parallel plate capacitor, and is typically large when the sample is more than a few unit cells thick. A "polar catastrophe" (i.e., a divergent electrostatic energy as the sample becomes macroscopically thick) is avoided by a transfer of charge between the two surfaces. This screening charge eliminates the potential difference across the film, but changes the doping at the surfaces and leads to the formation of surface states. The existence of surface states in YBCO has recently been confirmed by angle resolved photoemission (ARPES) experiments.[19,20]

The second aspect of YBCO that makes it distinct from BSCCO is the presence of layers of one-dimensional CuO chains, in addition to the CuO_2 plane bilayers. The naive view is that these chains carry charge in parallel to the CuO_2 bilayers, but have little direct impact on the CuO_2 layers. The chains are, therefore, generally ignored in models of YBCO.

For in-plane transport experiments, this point of view appears justified since it is possible to eliminate the effects of the chains (which run parallel to the *b* axis) by measuring transport in the *a*-axis direction; however, the chains are not easily disentangled from most other types of experiment. For example, *c*-axis currents (perpendicular to the planes) must pass through the CuO_2 and CuO layers in series, so that the *c*-axis resistivity is dominated by the Fermi surface mismatch between plane and chain layers.[21] As another example, CuO chains have been argued to cause an anomalous vortex core expansion at low magnetic fields in YBCO,[22] which is connected to a small superconducting energy scale in the chains.[23] In a similar vein, we find in this work that the effects of the chains are subtle, but are important for understanding some details of the density of states in the CuO_2 layers.

In this work, we calculate the tunneling DOS for a tight-binding model of YBCO that is based on recent experimental ARPES measurements of the band structure. There have, over the years, been many attempts to measure the YBCO spectrum using ARPES but, for reasons discussed above, it is difficult to do reliably. Some of the first successful measurements were made by Schabel *et al.*,[24,25] who found a complicated set of bands, not all of which could be easily related to bands predicted by density-functional theory (DFT) calculations. Later work by Lu *et al.*[26] identified an anisotropic spectrum consistent with the presence of CuO chains, and measurements in $YBa_2Cu_4O_8$ confirmed the existence of a pair of chain Fermi surfaces in that material.[27] Recent experiments by Zabolotnyy *et al.*[20] and Nakayama *et al.*[19] mapped out the Fermi surfaces of the surface states in some detail. Most recently Okawa *et al.*[28] have succeeded in imaging states in the bulk, and were able to partially map the Fermi surface and superconducting gap near the middle of the Brillouin zone.

The goal of this work is to develop a self-consistent model for surface and bulk states in $Y_{1-y}Ca_yBa_2Cu_3O_{7-\delta}$, and to use this model to understand details of the tunneling DOS. We remark that YBCO is sufficiently three-dimensional that it is not possible to model surface states by considering a single isolated CuO_2 layer, as is frequently done to model BSCCO. Instead, we develop a model for a *c*-axis oriented film of thickness N_c unit cells.

The approach we take is phenomenological. In Sec. II, we develop a model Hamiltonian for YBCO from least-squares fits of a tight-binding dispersion to the surface states measured in Ref. 19. We focus on optimal and overdoped YBCO, where we hope to avoid complications arising from competing phases or quantum critical points. The ARPES spectrum gives us the two-dimensional (2D) dispersion curves for the surface states; we assume that these dispersions are rigid, meaning that dispersions for bulk CuO_2 layers may be obtained by shifting the surface dispersions up or down in energy. This process allows us to infer the structure of the bulk bands based on the measured surface states. We find that the inferred bands agree with the measured bulk Fermi surface from Ref. 28. We then perform self-consistent calculations for the electrostatic potential in a finite-thickness film; this gives us the band-bending profile near the surfaces. We add superconductivity to the CuO_2 layers by hand, using a phenomenological relationship between the magnitude of the order parameter and the charge density. In this way, it is found that the order parameter is smaller on CuO_2-terminated surfaces than in the bulk. Finally, we calculate the superconducting DOS and normal state spectral functions for both surface and bulk layers. We discuss the results of these calculations in Sec. III. In this section, we conclude that, unlike in BSCCO, the density of states is sensitive to details of the band structure, and that these details naturally explain some of the features seen experimentally.

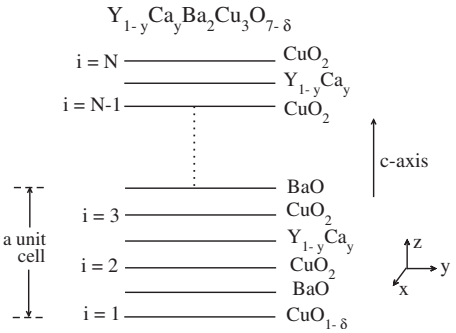

FIG. 1. Model of a Ca-doped YBCO thin film. The film is N_c unit cells thick, and each unit cell contains two superconducting CuO_2 and one conducting CuO layer, for a total of $N=3N_c$ conducting layers. The conducting layers are labeled $i=1,\ldots,N$, with $i=1$ corresponding to the chain-terminated surface, and $i=N$ corresponding to the CuO_2 plane-terminated surface. The CuO_2 and CuO layers are described by two- and one-dimensional dispersions $\xi_{ip}(\mathbf{k})$ and $\xi_{ic}(\mathbf{k})$, respectively, where $\mathbf{k}=(k_x,k_y)$ and are coupled by interlayer hopping matrix elements $t_{\perp p}$ (plane-plane) and $t_{\perp c}$ (chain-plane). The nonconducting layers are not included in the band structure calculations, although the Y/Ca layers are included in calculations of the electrostatic potential. The BaO layers are electrically neutral and are ignored. Results in this work are shown for $N_c=10$ unit cells.

II. METHOD

We consider a thin film consisting of N_c unit cells, stacked along their *c*-axis, as illustrated in Fig. 1. Each unit cell contains three conducting layers (two CuO_2 planes and one CuO chain layer) and three insulating layers (a $Y_{1-y}Ca_y$ layer and two BaO layers). The total number of conducting layers is therefore $N=3N_c$. Experimentally, it is known that YBCO cleaves at the BaO layer, so that the top conducting layer may be either a CuO chain layer or a CuO_2 plane layer. To study both cases, we assume that the first layer ($i=1$) is composed of CuO chains, and the last layer ($i=N$) is a CuO_2 plane.

Of the three nonconducting layers, two (the BaO layers) are nominally neutral and are not explicitly considered in the model. The yttrium and calcium atoms are nominally in the Y^{3+} and Ca^{2+} states and are retained in calculations of the long-ranged Coulomb potential.

Of the three conducting layers, it is assumed that only the CuO_2 planes are intrinsically superconducting, and that the

chains are superconducting because of their proximity to the planes. The proximity model for chain superconductivity has been discussed at length elsewhere.[29–32] The essential idea is that single-electron hopping between the chain and plane layers leads to mixing of the electronic wave functions, and to induced pairing in the chain layer.

The mean-field Hamiltonian of the system is

$$H = \sum_{\mathbf{k}} \hat{C}_{\mathbf{k}}^{\dagger} H_{\mathbf{k}} \hat{C}_{\mathbf{k}}, \tag{1}$$

where $\hat{C}_{\mathbf{k}}^{\dagger} = [\hat{c}_{1\mathbf{k}\uparrow}^{\dagger}, \hat{c}_{1-\mathbf{k}\downarrow}, \ldots, \hat{c}_{N\mathbf{k}\uparrow}^{\dagger}, \hat{c}_{N-\mathbf{k}\downarrow}]$ and $\hat{c}_{i\mathbf{k}\sigma}^{\dagger}$ is the creation operator for a spin-σ electron in the conducting layer i with 2D wave vector $\mathbf{k}=(k_x,k_y)$. $H_{\mathbf{k}}$ is given by

TABLE I. Parameters for the tight-binding model for YBCO. t_p, t', t'', t''', and $t_{\perp p}$ are found by fitting to ARPES experiments. t_c is estimated from DFT calculations and is roughly consistent with penetration depth anisotropy measurements (see text for details). There is no direct evidence for $t_{\perp c}$; the value shown below gives a reasonable fit to the measured tunneling DOS in optimally doped YBCO.

Parameter	Value
t_p	105 meV
t'	−0.277
t''	0.234
t'''	−0.042
t_c	500 meV
$t_{\perp p}$	61 meV
$t_{\perp c}$	$1.1t_{\perp p}$

$$H_{\mathbf{k}} = \begin{bmatrix}
\xi_{1c}(\mathbf{k}) & 0 & t_{\perp c} & & & & & & \\
0 & -\xi_{1c}(\mathbf{k}) & 0 & -t_{\perp c} & & & & & \\
t_{\perp c} & 0 & \xi_{2p}(\mathbf{k}) & \Delta_{2\mathbf{k}} & t_{\perp p} & & & & \\
 & -t_{\perp c} & \Delta_{2\mathbf{k}} & -\xi_{2p}(\mathbf{k}) & 0 & -t_{\perp p} & & 0 & \\
 & & t_{\perp p} & 0 & \xi_{3p}(\mathbf{k}) & \Delta_{3\mathbf{k}} & & & \\
 & & & -t_{\perp p} & \Delta_{3\mathbf{k}} & -\xi_{3p}(\mathbf{k}) & & & \\
 & 0 & & & & & \ddots & & -t_{\perp p} \\
 & & & & & & & \xi_{Np}(\mathbf{k}) & \Delta_{N\mathbf{k}} \\
 & & & & & & -t_{\perp p} & \Delta_{N\mathbf{k}} & -\xi_{Np}(\mathbf{k})
\end{bmatrix}, \tag{2}$$

where $\xi_{ic(p)}(\mathbf{k})$ is the 2D chain (plane) energy dispersion in conducting layer i. The matrix elements $t_{\perp c}$ and $t_{\perp p}$ are for plane-chain and plane-plane hopping, respectively. We remark that, in BSCCO, the plane-plane hopping matrix element has a strong $\mathbf{k}$ dependence; ARPES experiments[28] and DFT calculations[33] agree that the $\mathbf{k}$ dependence in YBCO is weaker, and we have neglected it here as a way of reducing the number of fitting parameters in our model.

For the intralayer dispersions, we use tight-binding models with nearest-neighbor and fourth-nearest neighbor hopping for the chains and planes, respectivley,

$$\xi_{ic}(\mathbf{k}) = -2t_c \cos k_y + \Phi_i, \tag{3}$$

$$\xi_{ip}(\mathbf{k}) = -2t_p[\cos k_x + \cos k_y + 2t' \cos k_x \cos k_y + t''(\cos 2k_x + \cos 2k_y) + 2t'''(\cos 2k_x \cos k_y + \cos 2k_y \cos k_x)] + \Phi_i, \tag{4}$$

where the values of t_c, t_p, t', t'', t''', and $t_{\perp p}$ are shown in Table I. The potential Φ_i includes short and long range Coulomb interactions, as well as offset potentials for the plane and chain layers, and the chemical potential. The method of calculating Φ_i is discussed below.

It is known that the superconducting order parameter in the CuO_2 planes has $d_{x^2-y^2}+s$ symmetry[34] as a result of the orthorhombic crystal structure. From experiments,[35] the s-wave component is approximately 15% of the d-wave component, and we assume that this ratio holds at both the surfaces and in the bulk. Denoting the d-wave and s-wave components in layer i by Δ_{id} and Δ_{is}, respectively, we have

$$\Delta_{i\mathbf{k}} = \begin{cases} \frac{\Delta_{id}}{2}[\cos(k_x) - \cos(k_y)] + \Delta_{is}, & i \in \text{plane} \\ 0, & i \in \text{chain}. \end{cases} \tag{5}$$

Note that, although the order parameter is zero in the chains, superconductivity is induced by the proximity effect. We adopt the phenomenological expression for Δ_{id} in the CuO_2 layers

$$\Delta_{id} = \frac{100[n_i - n_{\min}]}{1 - n_{\min}} \text{ meV}, \tag{6}$$

where n_i is the charge density in plane i and $n_{\min}=0.7$. We expect Eq. (6) to be valid on the overdoped side of the phase

diagram. At optimal doping (with planar charge density $n_p \approx 0.84$ in the bulk), this gives a d-wave order parameter of magnitude 46 meV, which is close to values inferred from recent ARPES measurements.[28] Eq. (6) also implies that the gap vanishes when the electron concentration is less than $n_{\min}$. The value of $n_{\min}$ is not well known and is probably material dependent (depending, for example, on the level of doping-related disorder); the canonical form for $La_{2-x}Sr_xCuO_4$ gives $n_{\min}=0.73$, but tunneling experiments[4] on $Y_{1-y}Ca_yBa_2Cu_3O_{7-\delta}$ suggest that superconductivity is still present at this doping level in YBCO. Our choice seems reasonably consistent with these experiments.

The potentials in Eqs. (3) and (4) are calculated from a self-consistent mean-field treatment. We write

$$\Phi_i = \begin{cases} \phi_i + \epsilon_p, & i \in \text{plane} \\ \phi_i + \epsilon_c, & i \in \text{chain}. \end{cases} \tag{7}$$

where ϕ_i is the electrostatic potential, and $\epsilon_{c(p)}$ includes the chemical potential and the energy of the chain (plane) tight-binding orbitals. We determine ϵ_p and ϵ_c by specifying the bulk plane and chain charge densities at optimal doping ($\delta=0.08$), which we take to be $n_p=0.84$ and $n_c=0.48$ electrons per 2D unit cell, respectively. Note that, once n_p is chosen, n_c is set by the constraint of charge neutrality, given by Eq. (11) below. Our self-consistent calculations then find $\epsilon_c-\epsilon_p=3.176$ eV at optimal doping. We assume that the tight-binding orbitals are not modified by doping, so that $\epsilon_c-\epsilon_p$ is held constant throughout this work. In our calculations chemical doping modifies the band structure only through the electrostatic potential ϕ_i.

The Coulomb potential ϕ_i is then calculated self-consistently within the Hartree approximation, under the assumption that the charge is uniformly distributed within each layer. For the planar geometry shown in Fig. 1,

$$\phi_i = \begin{cases} -\kappa \sum_j \sigma_j |z_i - z_j| + U\dfrac{n_i}{2}, & i \in \text{plane} \\ -\kappa \sum_j \sigma_j |z_i - z_j|, & i \in \text{chain}, \end{cases} \tag{8}$$

where the $Y_{1-y}Ca_y$ layers are implicitly included in the sum over j and

$$\kappa = \frac{2\pi e^2 d_z}{\epsilon a_0^2}. \tag{9}$$

In Eq. (8), U is the intraorbital Coulomb potential for the CuO_2 layers, which we take to be 4 eV. The total 2D charge density in layer i is $\sigma_i=Z_i-n_i$, where Z_i is the charge density of the ionic cores. Here, n_i is measured relative to the Cu^{3+} and O^{2-} states, so that

$$\sigma_j = \begin{cases} 1+2\delta-n_j, & j \in CuO_{1-\delta} \text{ chain} \\ -1-n_i, & j \in CuO_2 \text{ plane} \\ 3-y, & j \in Y_{1-y}{}^{3+}Ca_y{}^{2+} \text{ layer}. \end{cases} \tag{10}$$

All charge densities are in units of e/a_0^2, where $a_0 \approx 4$ Å is the 2D lattice constant. Electrical neutrality requires that

$$n_c + 2n_p = 2 + 2\delta - y. \tag{11}$$

In Eq. (8), z_i is the z coordinate of layer i, in units of the c-axis lattice constant $d_z \approx 12$ Å. Within a unit cell, the layers are at $z=0$ (chain), $z=0.354$ (first plane), $z=0.5$ (Y layer), and $z=0.646$ (second plane).[36] The weak doping dependence of these values is ignored here. The dielectric constant ϵ in Eq. (8) is not well known, but is believed to be around $\epsilon=20$, which is the value taken here.

For a given potential Φ_i, the charge density in layer i is found from the eigenvalues $E_{\alpha,\mathbf{k}}$ and eigenstates $\Psi_{\alpha,\mathbf{k}}(i,\sigma)$ of $H_{\mathbf{k}}$ via

$$n_i = \frac{2}{N_k}\sum_{\mathbf{k}} \sum_{\alpha=1}^{2N} |\Psi_{\alpha,\mathbf{k}}(i,\uparrow)|^2 f(E_{\alpha,\mathbf{k}}), \tag{12}$$

where $f(x)$ is the Fermi function, the factor of 2 is for spin, and N_k is the number of k points in the sum. The band index α ranges from 1 to $2N$ because the number of bands in the film is equal to twice (including spin) the number of conducting layers. The updated charge density is used to recalculate Φ_i, which is then used in the next iteration for n_i. The iterations proceed until the difference between n_i in two consecutive iterations is less than 10^{-5}. To reduce the computational workload, Φ_i is calculated in the normal state.

We finish this section with a brief discussion of the fitting procedure used to get the model parameters shown in Table I. As discussed above, we fit the 2D dispersions for the CuO_2 layers to the surface states measured in Ref. 19. In order to avoid complications from the chains, we fit the energy spectrum for an isolated CuO_2 bilayer to the measured bands in regions of the Brillouin zone far from the chain Fermi surface. The model bilayer has bonding and antibonding bands, with energies $\xi^{\pm}(\mathbf{k})=\xi_p(\mathbf{k})\pm t_{\perp p}$, which allows us to determine t_p, t', t'', t''', and $t_{\perp p}$. One potential difficulty with this fitting process is that it assumes that the electrostatic potential is the same in the top two CuO_2 layers, meaning that we attribute the experimental bilayer splitting entirely to $t_{\perp p}$. If we allow for a potential difference $\Delta\phi$ between the CuO_2 layers making up the bilayer (due to band bending at the surfaces), then $\xi^{\pm}(\mathbf{k})=\xi_p(\mathbf{k})\pm\sqrt{(\Delta\phi/2)^2+t_{\perp p}^2}$. Self-consistent calculations reported in the next section suggest $\Delta\phi \sim 10$ meV while the measured $t_{\perp p} \approx 60$ meV; it follows that $\Delta\phi$ modifies the band energies by less than 1% and can safely be neglected.

There are, at present, no reliable measurements of the chain band structure. However, there are good reasons to believe that the chain bands are only weakly renormalized by strong correlations. On theoretical grounds, we anticipate this because the chains are far from half filling. Within the Gutzwiller approximation,[37] the effective mass renormalization is $m/m^*=2p/(1+p)$ where $p=1-n$ is the hole concentration measured relative to half filling. For $n_c \sim 0.4$, we have $m/m^* \sim 0.75$, compared with $m/m^* \sim 0.27$ for $n_p=0.84$ in the CuO_2 layers. Experimentally, the strongest evidence for a small effective mass in the chains comes from the penetration depth anisotropy $\lambda_a^2/\lambda_b^2 \sim 2.4$ in YBCO.[38] Accounting for the presence of two CuO_2 layers for each CuO chain, this suggests that the chain effective mass is approximately 2.8

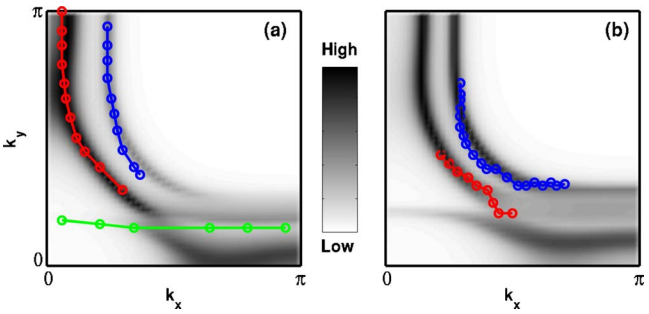

FIG. 2. (Color online) Comparison of the self-consistently calculated spectral function at ε_F to the experimentally measured Fermi surface (circles). Results are for (a) surface states (data from Ref. 19) and (b) bulk states (data from Ref. 28).

times larger than in the planes. We take a chain bandwidth of ~2 eV, which is roughly 2.5 times larger than the CuO_2 bandwidth $\sim 8t_p$. This gives the intrachain hopping matrix element $t_c \sim 500$ meV.

The hardest parameter to establish is $t_{\perp c}$, the chain-plane coupling. We show results for multiple values of $t_{\perp c}$ in Sec. III B, and find that the experimental density of states is reasonably well fit for $t_{\perp c}=1.1t_{\perp p}$ for $YBa_2Cu_3O_{6.92}$.

We show the results of our fitting procedure in Fig. 2. In this figure, we compare calculated surface and bulk spectral functions at the Fermi energy with the surface and bulk spectral functions measured by ARPES. The calculations are in good agreement with the experiments, which suggests that the assumptions made in developing our model are reasonable.

III. RESULTS AND DISCUSSION

A. Self-consistent potential, charge density, and superconducting order parameter

Figure 3 shows the results of self-consistent calculations for the charge density and electrostatic potential. We take the specific case of $Y_{1-y}Ca_yBa_2Cu_3O_{6.92}$, which corresponds to optimal doping when $y=0$ and to overdoping when $y>0$. The self-consistently determined charge density is shown in Fig. 3(a) as a function of layer index i. (Recall that the layer indices $i=1$ and $i=30$ label the CuO chain-terminated and the CuO_2 plane-terminated surfaces, respectively.) As discussed in the introduction, Fig. 3(a) shows that there is charge transfer from the plane-terminated surface to the chain-terminated surface. This charge screens the electric field produced by the polar unit cells, so that the electric potential is constant across the thin film except near the surfaces. This is shown in Figs. 3(c) and 3(d). In these figures, we have plotted the difference

$$\Delta\Phi_{ip(c)} = \Phi_i - \Phi_{p(c)}, \tag{13}$$

between the potential in layer i and the potential for a plane (chain) in the bulk in order to make the comparison between different y values simpler. $\Delta\Phi_{ip(c)}$ is nonzero within a screening length of the surfaces and is positive (negative) at the plane (chain) surface. The charge density on the plane

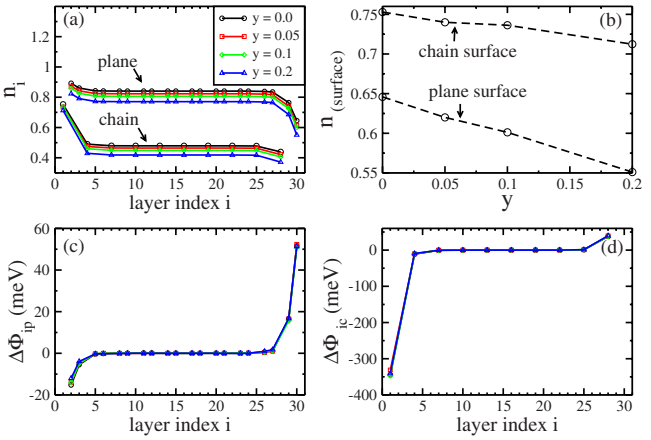

FIG. 3. (Color online) Self-consistent solutions for the charge density and electrostatic potential in $Y_{1-y}Ca_yBa_2Cu_3O_{6.92}$. Charge density is shown (a) for all CuO chain and CuO_2 plane layers in the thin film as a function of the layer index i, and (b) at the chain ($i=1$) and plane ($i=30$) surfaces as a function of y. The potential difference $\Delta\Phi_{ip(c)}=\Phi_i-\Phi_{p(c)}$, between the potential in layer i and the potential in the bulk planes (chains), is shown in (c) and (d).

(chain) surface is correspondingly smaller (larger) than in the bulk as shown in Fig. 3(a).

We note that $\Delta\Phi_{1c}$, the potential shift at the chain-terminated surface, is roughly seven times larger than $\Delta\Phi_{30p}$, the potential shift at the plane-terminated surface. This ratio is approximately the same as the ratio of the plane and chain densities of states (in the normal state); because of the small density of states in the chains, a large chemical potential shift is required at the chain-terminated surface to accommodate the charge transferred from the plane-terminated surface.

Figure 3 also shows the effect of Ca substitution. Despite the proximity of the Ca ions to the CuO_2 layers, n_i changes by roughly the same amount in both the CuO_2 and CuO layers. The one notable exception to this is at the chain surface, where the electron concentration changes by roughly half as much as in the bulk [Fig. 3(b)].

Figure 4 shows the d-wave superconducting order parameter Δ_{id} as a function of layer index i in the CuO_2 plane layers, and for different levels of Ca doping. Because Δ_{id} is calculated phenomenologically from Eq. (6), it follows n_i. Thus, Δ_{id} is larger than in the bulk near the chain surface and smaller than in the bulk near the plane surface. In our calculations, Δ_{id} actually vanishes at the CuO_2 surface layer ($i=30$), although there is a spectral gap due to proximity coupling to the subsurface layers. Note that recent ARPES experiments,[19,20] found that the surface is nonsuperconducting, but tunneling experiments[1–7] found a clear superconducting gap at the surface. We will show in the next section that the size of the superconducting gap at the CuO_2 surface is sensitive to how the surface is prepared.

Figures 3 and 4 are for films with one chain-terminated and one plane-terminated surface. For completeness, we consider the possibility that both surfaces are of the same type. Self-consistent calculations are shown for a film with two CuO_2-terminated surfaces in Fig. 5(a). In contrast to the overdoping found in the preceding calculations, the CuO_2 surfaces in this case are heavily underdoped, to the point

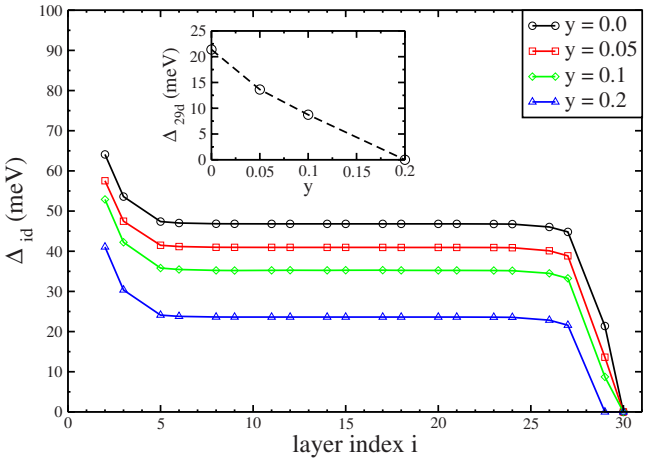

FIG. 4. (Color online) Superconducting order parameter as a function of layer index for $Y_{1-y}Ca_yBa_2Cu_3O_{6.92}$. The figure shows the d-wave component of the order parameter, which is nonzero in the CuO_2 layers only. The magnitude of Δ_{id} is given by Eq. (6). *Inset:* superconducting order parameter near the plane surface ($i=29$) as a function of Ca doping. Note that $\Delta_{30d}=0$.

where they lie in the Mott insulating region of the YBCO phase diagram. (Note that the result $n_i>1$ at the surfaces is an artifact of our calculations, which do not include Mott physics; the Mott gap will pin the charge density at $n_i=1$.) The DOS for this case should therefore be that of a featureless insulator. This kind of DOS is not reported in the literature, and we do not consider films of this type further.

For films with two chain-terminated surfaces, as in Fig. 5(b), the surface charge density is very similar to that found previously in Fig. 3. As a consequence, the DOS at the chain surface [Fig. 5(c)] is qualitatively indistinguishable from that reported in the next section for films with one chain-terminated and one plane-terminated surface. It is therefore not necessary to consider films of this type separately from films with both plane and chain surfaces, and we consider the latter for the remainder of this work.

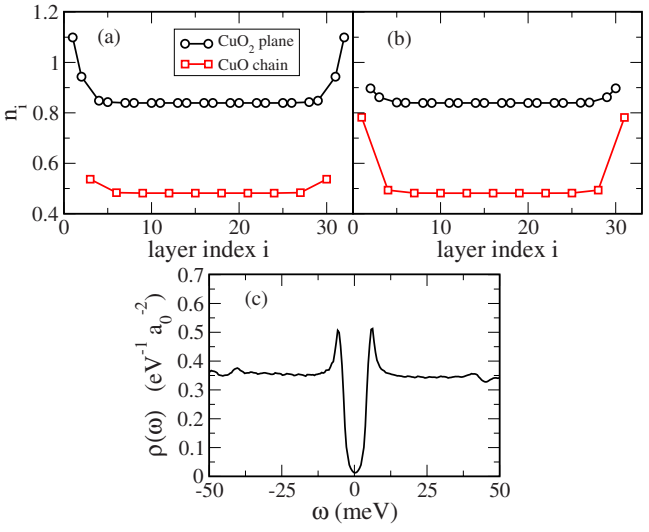

FIG. 5. (Color online) Results for films with identical surfaces. (a) Self-consistent charge density for a film whose terminating surfaces are both CuO_2 planes. Note that the surfaces should be Mott insulating based on their charge density. (b) Self-consistent charge density and (c) surface DOS for a film with two CuO-terminated surfaces.

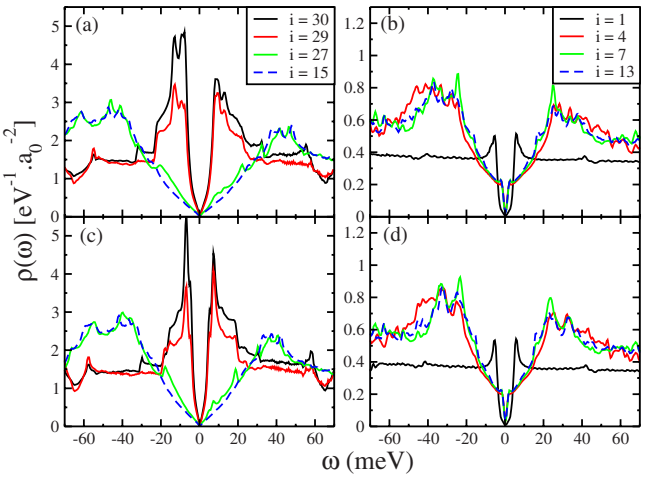

FIG. 6. (Color online) Surface and bulk density of states for $Y_{1-y}Ca_yBa_2Cu_3O_{6.92}$. Results are shown for $y=0.0$ [(a) and (b)] and for $y=0.05$ [(c) and (d)]. DOS is shown for CuO_2 planes [(a) and (c)] and CuO chains [(b) and (d)]. Model parameters are given in Table I. The bulk DOS ($i=13$ and $i=15$) is essentially the same as that of a uniform three-dimensional system with the same band parameters. Results are for $N_c=10$ and we have checked that the DOS is essentially unchanged for larger N_c.

B. Density of states and spectral function

The main results reported in this work are for the layer-dependent density of states and spectral function. The density of states at energy ω in layer i is given by

$$\rho_i(\omega) = \frac{1}{N_{\mathbf{k}}}\sum_{\mathbf{k}} A_i(\mathbf{k},\omega), \tag{14}$$

where $N_{\mathbf{k}}$ is the total number of $\mathbf{k}$ points, and $A_i(\mathbf{k},\omega)$ is spectral function in layer i,

$$A_i(\mathbf{k},\omega) = \sum_{\alpha=1}^{2N} [|\Psi_{\alpha,\mathbf{k}}(i,\uparrow)|^2\delta(\omega - E_{\alpha,\mathbf{k}}) + |\Psi_{\alpha,\mathbf{k}}(i,\downarrow)|^2\delta(\omega + E_{\alpha,\mathbf{k}})]. \tag{15}$$

Note that the eigenstates $\Psi_{\alpha,\mathbf{k}}(i,\sigma)$ and eigenenergies $E_{\alpha,\mathbf{k}}$ describe superconducting Bogoliubov quasiparticles with pseudospin index σ. In the nonsuperconducting state, the quasiparticles reduce to spin-up electrons ($\sigma=\uparrow$) with momentum $\mathbf{k}$, or spin-down holes ($\sigma=\downarrow$) with momentum $-\mathbf{k}$. In this work, all results for $A_i(\mathbf{k},\omega)$ are shown for the normal state at $\omega=\varepsilon_F$, while results for $\rho_i(\omega)$ are shown in the superconducting state.

Results for $Y_{1-y}Ca_yBa_2Cu_3O_{6.92}$ with $y=0$ and $y=0.05$ are shown in Fig. 6. This figure shows that the density of states at the surfaces is very different from in the bulk, for both the CuO_2 planes and CuO chains. Notably, the d-wave gap is significantly smaller at the surfaces than in the bulk. In the

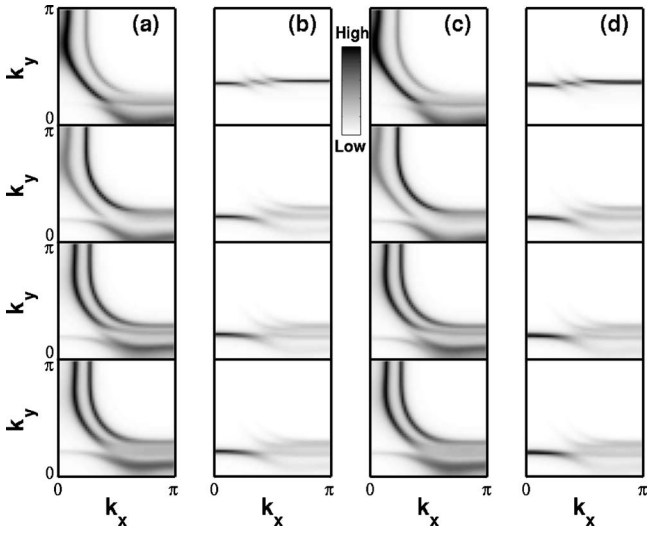

FIG. 7. Spectral function at the surfaces and in the bulk of $Y_{1-y}Ca_yBa_2Cu_3O_{6.92}$. Columns show $A(\mathbf{k},\varepsilon_F)$ for $y=0$ for (a) planes and (b) chains, and for $y=0.05$ for (c) planes and (d) chains. Rows (top to bottom) show layers $i=30$, 29, 27, 15 (planes) and $i=1$, 4, 7, 13 (chains); thus, surface states are shown in the top row, states deep in the bulk are shown in the bottom row.

CuO_2 layers, this reflects the suppression of Δ_{id} near the surface due to the decreased electron density in the surface layers. This is consistent with bulk-sensitive ARPES experiments that found a gap of order 42 meV,[28] and surface-sensitive tunneling experiments, which consistently find that the gap is $\lesssim 25$ meV.[1–7] In the chain layers, the reduced gap at the surface reflects the reduced proximity coupling at the chain surface, in part because the chain has only one nearest neighbor CuO_2 plane. Our calculation shows that the DOS obtains its bulk value within a few layers of either surface.

We note that, relative to the conventional model of a single-layer *d*-wave superconductor, the DOS in Fig. 6 shows a lot of structure. In particular, the CuO_2 surface (for $y=0$) has a main gap of about 10 meV, whose coherence peaks are split into pairs of closely spaced peaks, and a satellite "shoulder" at about 20 meV. Shoulder features have been commonly observed in tunneling experiments, and have been attributed to pairing,[4] and to competing order.[6] In our calculations, this structure comes from the interplay of pairing and band structure effects, namely the mixing of chain and plane states resulting in an orthorhombic distortion of the Fermi surfaces. This is illustrated in Fig. 7, which shows the layer-resolved spectral function $A_i(\mathbf{k},\varepsilon_F)$ at the Fermi energy. We see from this figure that chain-plane coupling strongly distorts the Fermi surfaces in the $(\pi,0)$ region of the Brillouin zone. This distortion is particularly important for the CuO_2 layers, because there is a van Hove singularity near the $(\pi,0)$ point in the undistorted spectrum. The DOS is therefore sensitive to small changes in the Fermi surface shape, caused either by chain-plane coupling, by doping, or by band-bending (changes in the electrostatic potential) near the surfaces. Thus, the addition of 5% Ca changes the electron density by only ~ 0.02 electrons per CuO_2 plaquette but qualitatively changes the shape of the coherence peaks [compare Figs. 6(a) and 6(c)]; in Fig. 7, we see that the main effect on the CuO_2 surface layer ($i=30$) is indeed near the $(\pi,0)$ point, where the spectral weight is reduced by Ca doping.

In Fig. 7, the intensity of $A_i(\mathbf{k},\omega)$ strongly depends on the amount of hybridization between chain and plane states. The Fermi surface at the CuO-terminated surface ($i=1$) is relatively undistorted, indicating weak chain-plane coupling. By contrast, the chain Fermi surface in the bulk is more strongly hybridized to the CuO_2 plane states and is correspondingly washed out. This is a possible reason that the chain Fermi surface was imaged in surface-sensitive ARPES measurements[19,20] but not in bulk-sensitive measurements.[28]

We remark that the amount of hybridization between chains and planes is strongly $\mathbf{k}$ dependent, even though the matrix element $t_{\perp c}$ is independent of $\mathbf{k}$. This is because the hybridization at each $\mathbf{k}$ depends on the energy difference between the chain and plane bands at that value of $\mathbf{k}$. Because these bands have different symmetries, the energy difference (and thus the hybridization) is a strong function of $\mathbf{k}$. It follows that the amount of hybridization at ε_F is a strong function of the relative positions of chain and plane Fermi surfaces, with the hybridization being largest where the Fermi surfaces cross. This explains the difference between the surface ($i=1$) and bulk ($i=13$) spectral functions shown in Fig. 7. A more extensive discussion of this point can be found in Ref. 31.

The degree to which the chain and plane Fermi surfaces hybridize determines the size of the induced gap in the chain layers. The small gap at the CuO surface (Fig. 6) is thus due to the weak hybridization of the surfaces chains with the underlying CuO_2 planes. In the bulk, the chain DOS shown in Fig. 6 has a main gap of about 20 meV, and a small gap of about 4 meV. The small gap originates from sections of the chain Fermi surface that are only weakly coupled to the planes (namely, $k_x \lesssim 1$) while the large gap comes from sections of the Fermi surface that are strongly coupled to the planes ($k_x \gtrsim 1$). The small gap was discussed previously as a possible source for the subgap structure measured in some tunneling experiments.[4]

Having discussed general features of the DOS and spectral function, we now discuss how these are affected by changes in specific model parameters. First, we allow for the possibility that the surface layers of the YBCO thin film are doped by the adsorption of atoms or molecules onto the surfaces. Adsorption happens naturally, for example, when YBCO is exposed to air, and deliberate potassium adsorption has been used to control the electron concentration in CuO_2 surface states.[39] In this work, we are interested in the possibility that the adsorbate layers partially screen the electric fields at the YBCO surfaces. We model this by assuming that the adsorbed layer has an average charge density of $+en_s$ ($-en_s$) at the CuO_2 (CuO) surface, where $n_s>0$. In our self-consistent calculations, the effect of the adsorbate charge is to dope the surface layers.

Figure 8 shows the effect of n_s on the density of states and spectral function. We see that even a relatively small adsorbate charge density has a significant effect on both $\rho_i(\omega)$ and $A_i(\mathbf{k},\omega)$ at the surfaces. In particular, $\rho_i(\omega)$ and $A_i(\mathbf{k},\omega)$ at the surfaces are increasingly similar to the bulk as n_s increases. This follows directly from the fact that the charge

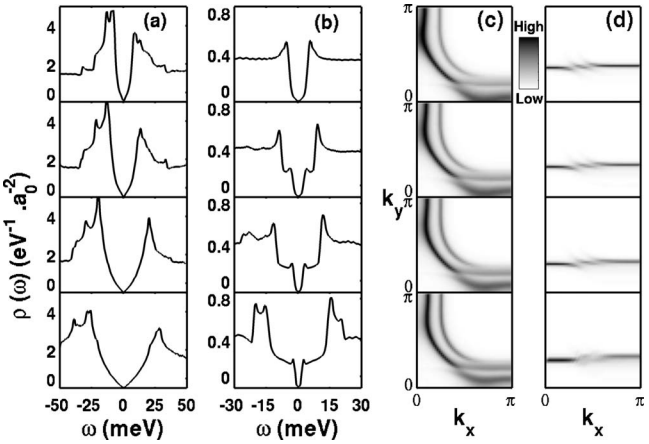

FIG. 8. Effects of an adsorbed surface layer on the surface states of $YBa_2Cu_3O_{6.92}$. Columns are for (a) plane and (b) chain DOS, (c) plane and (d) chain spectral function. The adsorbate layer has a 2D charge density of $+en_s$ for the CuO_2 surface and $-en_s$ for the CuO surface. Rows correspond to n_s=0.0, 0.1, 0.15, and 0.2 (top to bottom).

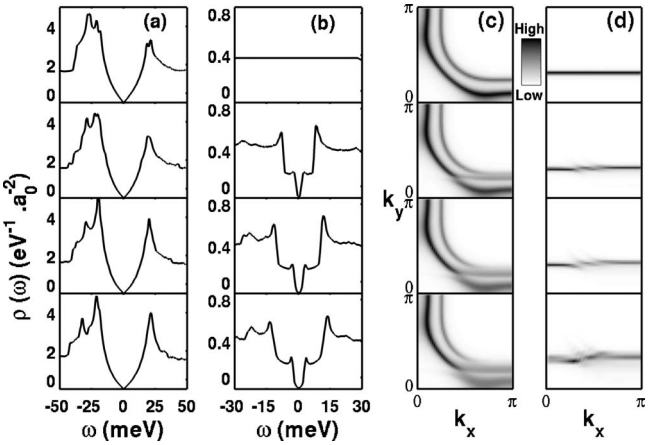

FIG. 9. Effects of chain-plane coupling on the surface states of $YB_2Cu_3O_{6.92}$. Columns are for (a) plane and (b) chain DOS and (c) plane and (d) chain spectral function. The adsorbate charge density is n_s=0.15. Rows correspond to $t_{\perp c}=0.0, 0.8t_{\perp p}, 1.1t_{\perp p}, 1.3t_{\perp p}$ (top to bottom).

densities at the surfaces approach their bulk values as n_s increases. In the CuO_2 layers, this results in a larger Δ_{id} from Eq. (6), while in the CuO layers, this results in an increased hybridization between the surface chains and the adjacent CuO_2 plane.

The CuO_2 spectrum for n_s=0.15 shown in Fig. 8 is consistent with existing tunneling experiments on optimally doped YBCO. For this case, we obtain coherence peaks at the CuO_2 surface at ± 20 meV and a satellite peak at ≈ -30 meV, in approximate agreement with Refs. 2, 6, and 8 (when comparing with experiments, recall that a peak at negative energy in the DOS corresponds to a peak at positive voltage bias in a tunneling experiment). We note that having a charged adsorbate layer is not the only way to obtain agreement with experiments; a different value for the dielectric constant, for example, will affect the surface charge density, and consequently the DOS. Whether or not our model is correct in all details, it demonstrates that existing tunneling measurements on optimally doped YBCO can be explained within a band picture.

Throughout this work, we have assumed that the plane-chain coupling parameter is $t_{\perp c}=1.1t_{\perp p}=67$ meV. This is the hardest of the model parameters to establish, and was chosen because it gives reasonable results for $\rho_i(\omega)$ and $A_i(\mathbf{k},\omega)$. Figure 9 shows the effect of varying $t_{\perp c}$ on the density of states and spectral function. Not surprisingly, chain-plane coupling has little effect on the DOS at the CuO_2 surface, apart from a shift of a weak negative-energy satellite peak away from the Fermi energy with increasing $t_{\perp c}$. In contrast, the chain surface is strongly influenced by coupling to the CuO_2 layer; the CuO chains are nonsuperconducting when $t_{\perp c}=0$, and an induced superconducting gap appears when $t_{\perp c}$ is nonzero. The induced gap grows approximately linearly with $t_{\perp c}$ and has both a subgap and a main gap, as discussed earlier. The spectral function also changes with increasing $t_{\perp c}$, becoming increasingly distorted near $(\pi,0)$.

Finally, we look more closely at the effects of Ca doping. In Ngai *et al.*,[4] samples with up to 20% Ca substitution for Y were studied, while in Yeh *et al.*,[3] 30% Ca-doped samples were studied. In Fig. 10, we show a series of calculations for the surface DOS of a $Y_{1-y}Ca_yBa_2Cu_3O_{6.92}$ thin film. Results are shown for both $n_s=0$ and n_s=0.15. The corresponding spectral functions are shown in Fig. 11.

As discussed above, the DOS exhibits subgap, main gap, and satellite features. In Ngai *et al.*, the three features were attributed to superconductivity on different regions of the Fermi surface. This is generally consistent with our findings here although we have found it difficult to attribute some satellite peaks to specific Fermi surface elements. Experimentally, the ratio between the satellite, main gap, and subgap energies was found to be approximately constant as a function of Ca doping, and this was argued to show that there is a common pairing mechanism for all three features. In our

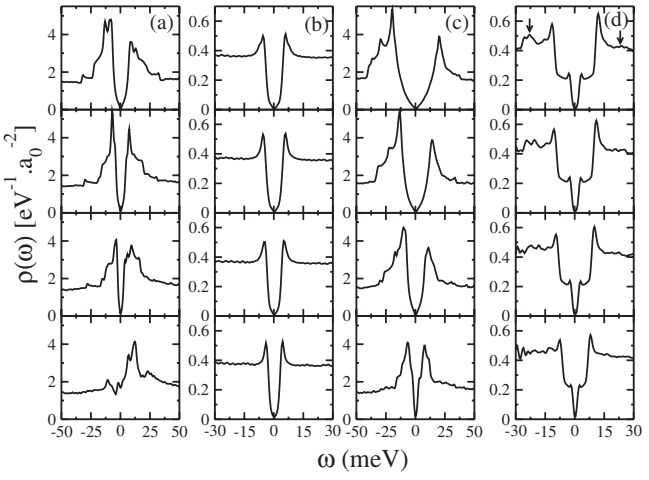

FIG. 10. Effects of Ca doping on the density of states of $Y_{1-y}Ca_yBa_2Cu_3O_{6.92}$ at the surfaces. Columns are for (a) plane and (b) chain surfaces with n_s=0.0, and (c) plane and (d) chain surfaces with n_s=0.15. Rows correspond to $y=0.0, 0.05, 0.10, 0.2$ (top to bottom). Arrows in (d) indicate the locations of satellite features discussed in the text.

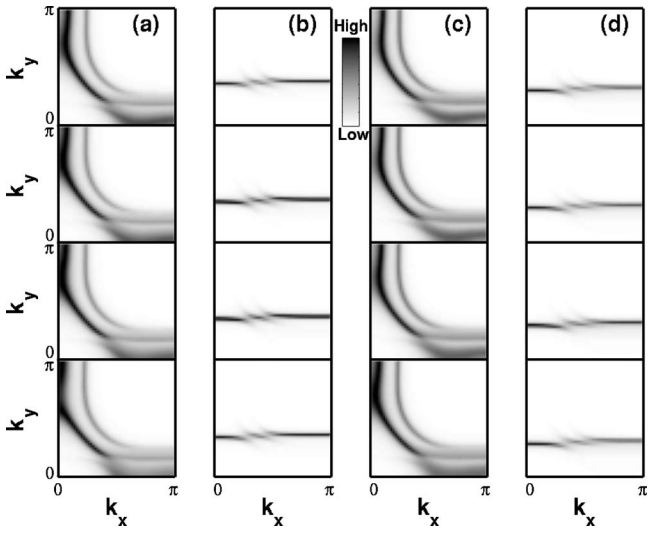

FIG. 11. Effect of Ca doping on the spectral function at the surfaces of $Y_{1-y}Ca_yBa_2Cu_3O_{6.92}$. Columns are for $n_s=0.0$ for (a) planes and (b) chains, and for $n_s=0.15$ for (c) planes and (d) chains. Rows are for $y=0.0, 0.05, 0.10, 0.2$ (top to bottom).

model the energies of the satellite and subgap features in Fig. 10 also scale with the main gap.

In some cases, our calculations reproduce the detailed structure of the experimental spectra. For $y=0.05$, Ngai *et al.* showed two types of spectrum. The first is remarkably similar to that shown for $y=0.05$ in Fig. 10(c), having pronounced coherence peaks and satellite features resembling shoulders. Spectra of this type are also measured in optimally doped ($y=0$) samples.[2,4,6,8] The good agreement between our calculations and the measured spectra suggests that our model captures the essential physics of the surface states in optimally doped YBCO.

The second type of measured spectrum qualitatively resembles that shown for $y=0.0$ in Fig. 10(d), having weak coherence peaks, a subgap feature, and satellite peaks (indicated by arrows in Fig. 10). However, there is a discrepancy between our calculations and the experiments; at higher Ca doping levels, the measured spectra continue to exhibit three sets of peaks while the satellite peaks in our calculations become less prominent. Given the sensitivity of the DOS to small changes in the model parameters, it is plausible that this discrepancy can be corrected by small changes to the model. It is also possible that extrinsic effects not considered here, for example tunneling matrix elements that emphasize the $(\pi,0)$ and $(0,\pi)$ regions of the Brillouin zone,[40,41] could increase the prominence of the satellite features in tunneling experiments. However, we also cannot rule out the possibility that our simple model for Ca substitution is overly naive.

Another feature of the DOS that is not explained by our model is the large residual DOS measured experimentally; the DOS is never seen to vanish at ε_F in the superconducting state, and is often 50% of the normal state DOS. It is not clear whether the residual DOS is intrinsic (for example, due to pair breaking at the surface) or extrinsic (coming from surface states in an adsorbate layer). It is possible that a full description of the YBCO surface states will require a proper accounting of this residual DOS.

IV. CONCLUSIONS

We have studied the surface and bulk states of $Y_{1-y}Ca_yBa_2Cu_3O_{6.92}$ with $0<y<0.2$ within a tight-binding model. The model parameters for the CuO_2 planes are extracted from photoemission experiments, and self-consistent calculations are used to relate the surface and bulk states. We have calculated the density of states $\rho_i(\omega)$ and spectral function $A_i(\mathbf{k},\varepsilon_F)$ as functions of adsorbed surface charge density, chain-plane coupling, and Ca doping. Our main findings are that

(i) our model produces results which are in simultaneous agreement with surface and bulk ARPES measurements. This supports two key assumptions of the model, that the surface and bulk bands are connected by a simple chemical potential shift and that the Coulomb potential can be treated in a planar approximation.

(ii) the DOS in optimally doped YBCO can be quantitatively explained by our model. In particular, shoulders measured in the density of states that were previously attributed to pairing or to competing order are found to be band structure effects.

(iii) the superconducting DOS is sensitive to small changes in the model parameters. This suggests that, in materials with CuO chains, small changes in doping of the surface states can have a qualitative effect on the density of states, purely as a result of changes to the band structure. This should be contrasted with BSCCO where it is believed that the doping dependence of the DOS is primarily due to strong correlations.

(iv) we can understand some features of Ca-doped YBCO; for example, our calculations find densities of states at the chain surface with subgap, main gap, and satellite features similar to experiments. However, we have not understood the dependence of this spectrum on Ca concentration.

ACKNOWLEDGMENTS

We would like to acknowledge helpful conversations with J. Mannhart, T. Kopp, J. Wei, and J. Ngai. K.P. thanks The Commission on Higher Education Grant, Thailand (Grant No. 12/2548) for financial support. This work was supported by NSERC of Canada and by SFB 484 from the DFG. This work was, in part, made possible by the facilities of the Shared Hierarchical Academic Research Computing Network (SHARCNET:www.sharcnet.ca) and Compute/Calcul Canada.

*billatkinson@trentu.ca

[1] J. M. Valles, R. C. Dynes, A. M. Cucolo, M. Gurvitch, L. F. Schneemeyer, J. P. Garno, and J. V. Waszczak, Phys. Rev. B **44**, 11986 (1991).

[2] I. Maggio-Aprile, C. Renner, A. Erb, E. Walker, and O. Fischer, Phys. Rev. Lett. **75**, 2754 (1995).

[3] N.-C. Yeh, C.-T. Chen, G. Hammerl, J. Mannhart, A. Schmehl, C. W. Schneider, R. R. Schulz, S. Tajima, K. Yoshida, D. Garrigus, and M. Strasik, Phys. Rev. Lett. **87**, 087003 (2001).

[4] J. H. Ngai, W. A. Atkinson, and J. Y. T. Wei, Phys. Rev. Lett. **98**, 177003 (2007).

[5] P. Das, M. R. Koblischka, H. Rosner, T. Wolf, and U. Hartmann, Phys. Rev. B **78**, 214505 (2008).

[6] A. D. Beyer, M. S. Grinolds, M. L. Teague, S. Tajima, and N.-C. Yeh, EPL **87**, 37005 (2009).

[7] O. Fischer, M. Kugler, I. Maggio-Aprile, C. Berthod, and C. Renner, Rev. Mod. Phys. **79**, 353 (2007).

[8] T. Cren, D. Roditchev, W. Sacks, and J. Klein, Europhys. Lett. **52**, 203 (2000).

[9] A. Beyer, C.-T. Chen, M. Grinolds, M. Teague, and N.-C. Yeh, Physica C **468**, 471 (2008).

[10] T. Cren, D. Roditchev, W. Sacks, J. Klein, J.-B. Moussy, C. Deville-Cavellin, and M. Laguës, Phys. Rev. Lett. **84**, 147 (2000).

[11] S. H. Pan, J. P. O'Neal, R. L. Badzey, C. Chamon, H. Ding, J. R. Engelbrecht, Z. Wang, H. Eisaki, S. Uchida, A. K. Gupta, K.-W. Ng, E. W. Hudson, K. M. Lang, and J. C. Davis, Nature (London) **413**, 282 (2001).

[12] C. Howald, P. Fournier, and A. Kapitulnik, Phys. Rev. B **64**, 100504(R) (2001).

[13] M. R. Norman, M. Randeria, H. Ding, and J. C. Campuzano, Phys. Rev. B **52**, 615 (1995).

[14] R. S. Markiewicz, S. Sahrakorpi, M. Lindroos, H. Lin, and A. Bansil, Phys. Rev. B **72**, 054519 (2005).

[15] Z. Yusof, J. F. Zasadzinski, L. Coffey, and N. Miyakawa, Phys. Rev. B **58**, 514 (1998).

[16] B. W. Hoogenboom, C. Berthod, M. Peter, O. Fischer, and A. A. Kordyuk, Phys. Rev. B **67**, 224502 (2003).

[17] N. Nakagawa, H. Y. Hwang, and D. A. Muller, Nature Mater. **5**, 204 (2006).

[18] S. Thiel, G. Hammerl, A. Schmehl, C. W. Schneider, and J. Mannhart, Science **313**, 1942 (2006).

[19] K. Nakayama, T. Sato, K. Terashima, H. Matsui, T. Takahashi, M. Kubota, K. Ono, T. Nishizaki, Y. Takahashi, and N. Kobayashi, Phys. Rev. B **75**, 014513 (2007).

[20] V. B. Zabolotnyy, S. V. Borisenko, A. A. Kordyuk, J. Geck, D. S. Inosov, A. Koitzsch, J. Fink, M. Knupfer, B. Büchner, S.-L. Drechsler, H. Berger, A. Erb, M. Lambacher, L. Patthey, V. Hinkov, and B. Keimer,Phys. Rev. B **76**, 064519 (2007).

[21] W. A. Atkinson and J. P. Carbotte, Phys. Rev. B **55**, 3230 (1997).

[22] W. A. Atkinson and J. E. Sonier, Phys. Rev. B **77**, 024514 (2008).

[23] N. D. Whelan and J. P. Carbotte, Phys. Rev. B **62**, 15221 (2000).

[24] M. C. Schabel, C.-H. Park, A. Matsuura, Z.-X. Shen, D. A. Bonn, R. Liang, and W. N. Hardy, Phys. Rev. B **57**, 6090 (1998).

[25] M. C. Schabel, C.-H. Park, A. Matsuura, Z.-X. Shen, D. A. Bonn, R. Liang, and W. N. Hardy, Phys. Rev. B **57**, 6107 (1998).

[26] D. H. Lu, D. L. Feng, N. P. Armitage, K. M. Shen, A. Damascelli, C. Kim, F. Ronning, Z.-X. Shen, D. A. Bonn, R. Liang, W. N. Hardy, A. I. Rykov, and S. Tajima, Phys. Rev. Lett. **86**, 4370 (2001).

[27] T. Kondo, *et al.*, Phys. Rev. Lett. **98**, 157002 (2007).

[28] M. Okawa, *et al.*, Phys. Rev. B **79**, 144528 (2009).

[29] M. Tachiki, S. Takahashi, F. Steglich, and H. Adrian, Z. Phys. B: Condens. Matter **80**, 161 (1990).

[30] C. O'Donovan and J. P. Carbotte, Phys. Rev. B **55**, 1200 (1997).

[31] W. A. Atkinson, Phys. Rev. B **59**, 3377 (1999).

[32] D. K. Morr and A. V. Balatsky, Phys. Rev. Lett. **87**, 247002 (2001).

[33] O. K. Andersen, A. I. Liechtenstein, O. Jepsen, and F. Paulsen, J. Phys. Chem. Solids **56**, 1573 (1995).

[34] X.-S. Ye and J.-X. Li, Phys. Rev. B **76**, 174503 (2007).

[35] H. J. H. Smilde, A. A. Golubov, Ariando, G. Rijnders, J. M. Dekkers, S. Harkema, D. H. A. Blank, H. Rogalla, and H. Hilgenkamp, Phys. Rev. Lett. **95**, 257001 (2005).

[36] G. Böttger, I. Mangelschots, E. Kaldis, P. Fischer, C. Krüger, and F. Fauth, J. Phys.: Condens. Matter **8**, 8889 (1996).

[37] F. Zhang, C. Gros, T. Rice, and H. Shiba, Supercond. Sci. Technol. **1**, 36 (1988).

[38] D. N. Basov, R. Liang, D. A. Bonn, W. N. Hardy, B. Dabrowski, M. Quijada, D. B. Tanner, J. P. Rice, D. M. Ginsberg, and T. Timusk, Phys. Rev. Lett. **74**, 598 (1995).

[39] M. A. Hossain, J. D. F. Mottershead, D. Fournier, A. Bostwick, J. L. McChesney, E. Rotenberg, R. Liang, W. N. Hardy, G. A. Sawatzky, J. S. Elfimov, D. A. Bonn, and A. Damascelli, Nat. Phys. **4**, 527 (2008).

[40] I. Martin, A. V. Balatsky, and J. Zaanen, Phys. Rev. Lett. **88**, 097003 (2002).

[41] J. Nieminen, H. Lin, R. S. Markiewicz, and A. Bansil, Phys. Rev. Lett. **102**, 037001 (2009).